Journal for ImmunoTherapy of Cancer

Glucocorticoid activation by HSD11B1 limits T cell-driven interferon signaling and response to PD-1 blockade in melanoma

Luiza Martins Nascentes Melo,[1,2] Dayana Herrera-Rios,[3,4] Daniel Hinze,[5] Stefanie Löffek,[1,2] Irem Oezel ,[6] Roberta Turiello,[5] Juliane Klein,[3,4] Sonia Leonardelli,[5] Isa-Vanessa Westedt,[1,2] Yahya Al-Matary,[1,2] Sara Egea-Rodriguez,[1,3,4] Alexandra Brenzel,[7] Maja Bau,[1,2] Antje Sucker,[1,2] Eva Hadaschik,[1] Florian Wirsdörfer,[8] Helmut Hanenberg,[9] Niklas Uhlenbrock,[10,11] Daniel Rauh,[10,11] Joanna Poźniak,[12,13] Florian Rambow,[1,2,12,13] Jean-Christophe Marine,[12,13] Maike Effern,[5] Nicole Glodde,[5] Dirk Schadendorf,[1,2] Jadwiga Jablonska ,[2,6] Michael Hölzel ,[5] Iris Helfrich [1,3,4]

To cite: Martins Nascentes Melo L, Herrera-Rios D, Hinze D, *et al*. Glucocorticoid activation by HSD11B1 limits T cell-driven interferon signaling and response to PD-1 blockade in melanoma. *Journal for ImmunoTherapy of Cancer* 2023;**11**:e004150. doi:10.1136/jitc-2021-004150

► Additional supplemental material is published online only. To view, please visit the journal online (http://dx.doi.org/10.1136/jitc-2021-004150).

LMNM, DH-R, DH and SL contributed equally.

MH and IH are joint senior authors.

Accepted 14 March 2023

Check for updates

For numbered affiliations see end of article.

Correspondence to
Dr Iris Helfrich;
Iris.Helfrich@med.uni-muenchen.de

Professor Michael Hölzel;
Michael.Hoelzel@ukbonn.de

ABSTRACT

Background Immune responses against tumors are subject to negative feedback regulation. Immune checkpoint inhibitors (ICIs) blocking Programmed cell death protein 1 (PD-1), a receptor expressed on T cells, or its ligand PD-L1 have significantly improved the treatment of cancer, in particular malignant melanoma. Nevertheless, responses and durability are variables, suggesting that additional critical negative feedback mechanisms exist and need to be targeted to improve therapeutic efficacy.

Methods We used different syngeneic melanoma mouse models and performed PD-1 blockade to identify novel mechanisms of negative immune regulation. Genetic gain-of-function and loss-of-function approaches as well as small molecule inhibitor applications were used for target validation in our melanoma models. We analyzed mouse melanoma tissues from treated and untreated mice by RNA-seq, immunofluorescence and flow cytometry to detect changes in pathway activities and immune cell composition of the tumor microenvironment. We analyzed tissue sections of patients with melanoma by immunohistochemistry as well as publicly available single-cell RNA-seq data and correlated target expression with clinical responses to ICIs.

Results Here, we identified 11-beta-hydroxysteroid dehydrogenase-1 (HSD11B1), an enzyme that converts inert glucocorticoids into active forms in tissues, as negative feedback mechanism in response to T cell immunotherapies. Glucocorticoids are potent suppressors of immune responses. HSD11B1 was expressed in different cellular compartments of melanomas, most notably myeloid cells but also T cells and melanoma cells. Enforced expression of HSD11B1 in mouse melanomas limited the efficacy of PD-1 blockade, whereas small molecule HSD11B1 inhibitors improved responses in a $CD8^+$ T cell-dependent manner. Mechanistically, HSD11B1 inhibition in combination with PD-1 blockade augmented the production of interferon-γ by T cells. Interferon pathway activation correlated with sensitivity to PD-1 blockade linked to anti-proliferative effects on melanoma cells. Furthermore, high levels of HSD11B1, predominantly expressed by tumor-associated macrophages, were associated with poor responses to ICI therapy in two independent cohorts of patients with advanced melanomas analyzed by different methods (scRNA-seq, immunohistochemistry).

Conclusion As HSD11B1 inhibitors are in the focus of drug development for metabolic diseases, our data suggest a drug repurposing strategy combining HSD11B1 inhibitors with ICIs to improve melanoma immunotherapy.

WHAT IS ALREADY KNOWN ON THIS TOPIC

⇒ The clinical success of immune checkpoint therapy in patients with malignant melanoma and other cancers has revolutionized the therapeutic landscape in metastatic cancer. However, massive immune-related adverse events leading to treatment discontinuation and limited response suggest a negative feedback mechanism that determines therapeutic efficacy and durability.

WHAT THIS STUDY ADDS

⇒ Inhibition of 11-beta-hydroxysteroid dehydrogenase-1 (HSD11B1) under PD-1 blockage supports a proinflammatory phenotype in tumor-associated macrophages promoting their ability to activate T cells in regulating interferon-γ-dependent immunity.

HOW THIS STUDY MIGHT AFFECT RESEARCH, PRACTICE OR POLICY

⇒ This study identified HSD11B1 as a novel enzymatic immune checkpoint in response to T cell immunotherapies in patients with malignant melanoma but also highlights the need for careful patient stratification with respect to the tumor immune landscape.

Furthermore, our work also delineated potential caveats emphasizing the need for careful patient stratification.

INTRODUCTION

Immune checkpoint inhibitors (ICIs) have substantially improved the treatment outcome of patients with melanoma.[1–3] ICIs are monoclonal antibodies that block cell surface molecules like PD-1 or cytotoxic T-lymphocyte-associated Protein 4 (CTLA-4) leading to reinvigoration of anti-tumor T cell immunity.[4] Despite high response rates, resistance to ICI therapy remains a clinical challenge and active field of research.[5–7] Recently, Grasso *et al*[8] performed transcription profiling of baseline and on-treatment biopsies from patients with advanced melanoma (CheckMate 038 study) receiving anti-PD-1 alone or in combination with anti-CTLA-4. The authors found that T cell infiltration and induction of interferon-γ (IFN-γ) signaling had the strongest predictive value for clinical responses to ICI therapy paralleled by melanoma cell growth arrest. Moreover, analyzing a panel of melanoma cell lines revealed a conserved response to IFN-γ, which was proposed to amplify the anti-tumor immune response within the tumor microenvironment (TME). Also, transcriptomic signatures linked to antigen presentation were found to be associated with favorable responses to ICI.[9]

Apart from IFN-γ, many signaling pathways or microenvironmental conditions influence anti-tumor immunity.[10] The role of glucocorticoids (GCs), however, tends to be neglected, even though their immunosuppressive functions are known for decades. GCs are frequently used to cope with immune-associated side effects generated by ICI claiming that anti-tumor effectivity is not harmed.[11–13] Primarily, GCs are produced in the adrenal cortex under the control of the hypothalamic–pituitary–adrenal axis, a neural-endocrine circuit coordinating metabolism and stress responses.[14] GC activity in target issues is regulated by intracellular enzymes, in particular 11-beta-hydroxysteroid dehydrogenase-1 (HSD11B1) that converts inactive GCs into active GCs,[15–17] a process of tissue-specific GC recycling and different from GC de novo synthesis. Recently, GC synthesis by tumor-associated myeloid cells and T cells has been implicated in the instruction of T cell dysfunction.[18 19]

Binding of GCs to the GC receptor (NR3C1, also known as GR), a ligand-activated transcription factor, and transcriptional regulation is considered as the classical mode of action.[20 21] GCs dampen proinflammatory cytokine production, leukocyte recruitment and activation including antigen-specific T cell responses.[14 22 23] Furthermore, GCs limit the maturation and activation of dendritic cells (DCs), a professional antigen presenting cell type centrally orchestrating T helper responses,[24] also relevant for cancer immunity.[25] Altogether, GCs exert immune regulation by a myriad of mechanisms, which are still not fully understood.

Here, we identified increased expression of HSD11B1 as a negative feedback mechanism of ICI therapy limiting IFN-γ signaling within melanomas. Pharmacological inhibition of HSD11B1 activity enhanced the efficacy of PD-1 blockade in a syngeneic melanoma mouse model dependent on $CD8^+$ T cells augmenting IFN-γ production. Furthermore, high expression of HSD11B1 predominantly by tumor-associated macrophages was associated with poor responses to ICI therapy in patients with melanoma. In the view of recent data by Grasso *et al*,[8] our data suggest to evaluate HSD11B1 inhibitors combined with ICIs to amplify IFN-γ signaling in melanomas and improve clinical responses.

MATERIALS AND METHODS

Patient-derived tissue samples

Formalin-fixed and paraffin-embedded (FFPE) tissue samples from metastases of patients with stage IV melanoma were used and classified regarding their best response toward anti-PD-1 monotherapy (progressive disease (PD) n=11; stable disease (SD) n=6; partial response (PR) n=4 and complete response (CR) n=3) according to the RECIST criteria. For 4 patients, matched pairs were taken before and under PD-1 inhibitor monotherapy using nivolumab or pembrolizumab were available that allowed for intraindividual comparative analysis. In total, we included 21 cutaneous, 2 nodal and 1 lung melanoma metastases in our study. The cohort and clinical data were provided by the Skin Cancer Biobank (SCABIO) of the Dermatology Department of the University Hospital Essen, Germany. All melanoma metastases were histopathologically diagnosed (EH).

Cell lines

Cutaneous melanoma (CM) and lymph node (LN) metastases) are cell lines generated from the *Mt-Ret* genetically engineered mouse melanoma model (GEMM).[26] HCmel12 melanoma cells were previously used in our studies[27 28] and originally provided by Thomas Tüting (now University Hospital Magdeburg, Germany).[29] B16F1 melanoma cells were purchased originally from American Type Culture Collection (ATCC). All melanoma cell lines were routinely cultured in 'complete RPMI medium', ie, RPMI 1640 medium (Gibco, #21875034) supplemented with 10% heat-inactivated fetal calf serum (FCS,PAA Laboratories), 2 mM L-glutamine (Gibco, #25030081); 100 IU/mL penicillin and 100 µg/mL streptomycin (Gibco, #15140122). The HEK293T cell line was purchased from ATCC and used for retrovirus production and routinely cultured in 'complete DMEM', that is, DMEM (Gibco, #41965039) supplemented with 10% heat-inactivated FCS (PAA Laboratories), 2 mM L-glutamine (Gibco); 100 IU/mL penicillin and 100 µg/mL streptomycin (Gibco). All cell lines were grown in a humidified incubator with 5% CO_2 at 37°C and tested for mycoplasma contamination on a monthly basis.

Generation of Hsd11b1-deficient cell lines

The Hsd11b1-deficient cell lines CM.*Hsd11b1*$^{-/-}$ and HCmel12.*Hsd11b1*$^{-/-}$ are based on a CRISPR-Cas9-mediated *Hsd11b1*-knockout in CM and HCmel12 melanoma cells. The plasmid pX330-U6-Chimeric_BB-CBh-hSpCas9 was digested with BbsI (New England Biolabs, #R0539L) and gel purified. A double-stranded DNA oligonucleotide (Microsynth) targeting the murine genome downstream of Hsd11b1 (K44) was cloned into the digested vector. The oligonucleotides used are listed in online supplemental table S5. The resulting plasmid pX330-*Hsd11b1*$^{-/-}$ was visualized by agarose gel electrophoresis and validated by Sanger sequencing (Microsynth). The CM and HCmel12 melanoma cells (3×10^5 cells; 12-well) were transfected with 2 µg of pX330-*Hsd11b1*$^{-/-}$ using FuGENE HD transfection reagent (Promega, #E2311) according to the manufacturer's instructions. Hsd11b1-deficient monoclones were grown from single-cell suspensions, validated by next generation sequencing (NGS) and analyzed using the web tool OutKnocker (http://www.outknocker.org/).[30] The plasmid pX330-U6-Chimeric_BB-CBh-hSpCas9 was a gift from Feng Zhang (Addgene plasmid #42230).

Generation of Hsd11b1-engineered cell lines

The *Hsd11b1*-engineered cell lines CM.pRP.*Hsd11b1*, CM.H*sd11b1*$^{-/-}$.pRP.*Hsd11b1* and HCmel12.*Hsd11b1*$^{-/-}$.pRP.*Hsd11b1* were generated by retroviral transduction of CM, CM.*Hsd11b1*$^{-/-}$ and HCmel12.*Hsd11b1*$^{-/-}$ melanoma cells with a pRP-based *Hsd11b1*-construct. The plasmid pRP was digested with BamHI-HF (New England Biolabs, #R3136L) and XhoI (New England Biolabs, #R0146L) and gel purified. The Hsd11b1 consensus CDS CCDS15635.1 (including a N-terminal BamHI-HF restriction site, a N-terminal Kozak sequence and a C-terminal XhoI restriction site) was amplified from CM-derived complementary DNA. The oligonucleotides used are listed in online supplemental table S6. The PCR product was purified, digested with BamHI-HF (New England Biolabs) and XhoI (New England Biolabs), purified and cloned into the digested vector. The resulting plasmid pRP.*Hsd11b1* was visualized by agarose gel electrophoresis and validated by Sanger sequencing (Microsynth). For retroviral transduction, HEK293T cells were cultured in complete DMEM and transfected with packaging plasmids (gag-pol and pCMV VSV-G) and pRP.*Hsd11b1* by calcium phosphate transfection. One day later, the HEK293T cells were washed with complete DMEM. One additional day later, the HEK293T supernatants were filtrated using a 0.45 µM syringe filter and added to the melanoma cells. Three additional days later, the melanoma cells were subjected to antibiotic selection with 2 µg/mL puromycin (Sigma-Aldrich, #P8833) for 3–4 days. The plasmid pRP was a gift from Eicke Latz (Institute of Innate Immunity, Bonn, Germany) (Addgene plasmid #41841). The plasmids gag-pol and pCMV VSV-G were also a gift from Eicke Latz (Institute of Innate Immunity).

Cell growth assays

For cell growth at low density, CM and LN melanoma cells (1500 cells; 12-well) were incubated for 24 hours with complete RPMI medium (Gibco) and afterwards treated with complete RPMI medium supplemented with recombinant murine IFN-γ (Peprotech, #315-05) at indicated concentrations or vehicle control for 6 or 8 days, respectively. The cells were fixed with 4% formaldehyde (Sigma-Aldrich, #47608) solution, washed with water, stained with 0.05% crystal violet (Sigma-Aldrich, #C0775) for 30 min and washed three times with water. Dry 12-well plates were scanned and quantified using the Odyssey SA Infrared Imaging System (LICOR Biosciences).

ELISA

ELISA was performed to evaluate the ability of Hsd11b1 to convert inactive 11-dehydrocorticosterone (11-DHCS) to active CS. CM, LN, B16F1 and HCmel12 melanoma cells (3×10^5 cells; 12-well) were incubated for 24 hours with complete RPMI medium, washed with PBS and incubated for up to 24 hours with FCS-free complete RPMI medium supplemented with DMSO (Carl Roth, #4720.1), 15.844 pg (0.046 µM) 11-DHCS (US Biological, #D3224-99) or 16.000 pg (≈ 0.046 µM) CS (Cayman Chemical, #16063). DMSO-containing, 11-DHCS-containing and CS-containing media were also incubated without cells and used as negative and positive controls. In case of Hsd11b1-inhibition FCS-free complete RPMI medium supplemented with DMSO (Carl Roth, #4720.1), Carbenoxolone (CBX, Sigma-Aldrich, #C4790) or 11beta-HSD1 inhibitor, 10j (Merck KGaA, #385581) was added 2 hours before GC treatment. Supernatants were collected and stored at −80°C. CS concentrations were determined using corticosterone (CS) ELISA kit (Enzo Life Sciences; #ADI-900-097) according to manufacturer's protocols. Samples were normalized as indicated.

In vivo tumorigenesis on anti-PD-1, CBX and 10j injections

In 200 µL Matrigel (Corning, #354277)/PBS (1:1) 5×10^5 CM cells were suspended and subcutaneously injected in 12-week-old C57BL/6 female mice. CBX (20 mg/kg, Sigma-Aldrich, #C4790), anti-PD-1 (10 mg/kg, clone RMP1-14, BioXcell, #BE0146) or isotype control IgG2a (10 mg/kg, clone 2A3, BioXcell, #BE0090) was intraperitoneally injected at days −1, 0, 2, 4, 6, 8 and 10 depending on the experimental setting. 10j (Merck KGaA, #385581) was subcutaneously injected at days −1, 0, 1 and 2 with a concentration of 10 µM/5% DMSO (Carl Roth, #4720.1) and at days 3, 4, 5, 6 and 7 with a concentration of 5 µM/2.5% DMSO. Five per cent DMSO in water was subcutaneously injected from day −1 to day 7 as a vehicle control. Animals were sacrificed on indicated time points. Tumor volumes were calculated using a caliper with the formula: tumor volume=width×length×height.

Isolation of CD8$^+$ T cells from CM melanoma

CD8$^+$ T cells were isolated from tumor single-cell suspensions using flow sorting (FACS Aria cell sorter, BD

Biosciences). Single-cell suspension from tumor tissues was incubated with PBS containing Mouse BD Fc Block, eBioscience Fixable Viability Dye eFluor 780 and anti-mouse CD8a Pacific Blue (558106, Clone: 53-6.7, Rat IgG2a, κ, BD Biosciences). $CD8^+$ T cells were sorted with the purity >90%.

Immune depletion of $CD8^+$ T cells

Anti-CD8a depleting antibody (40 mg/kg, clone 2.43, BioXcell, #BE0061) was intraperitoneally injected every 4 days starting from day −1 prior CM cells transplantation until mice were euthanized. IgG2a (10 mg/kg, clone 2A3, BioXcell, #BE0090) was used as its isotype control. CD8 depletion efficacy was validated in blood, draining LNs and tumors, with the indicated antibodies by flow cytometry (BD FACS Aria III, BD Biosciences).

Flow cytometry

Tumor tissues and LNs were harvested, digested and dissociated using the mouse tumor dissociation kit (mTDK) (Miltenyi Biotec, #130-096-730) and the gentleMACS Dissociator (Miltenyi Biotec) according to the manufacturer's instructions. Single-cell suspensions were passed through a 70 µm cell strainer (Falcon, #10788201) and washed twice with PBS (Gibco, #11503387). For the lysis of erythrocytes, blood and tumor suspensions were incubated with 1× RBC Lysis Buffer (BioLegend, #420301) for 5 min and washed twice with PBS before further processing. Single-cell suspensions were incubated with CD16/CD32 blocking antibody (1:200, BD Biosciences, #553142) prior to incubation with fluorochrome-conjugated antibodies. For analysis of live and dead cells, Zombie NIR Fixable Viability Dye Kit (1:1000, BioLegend, #423105) was used. Fluorochrome-conjugated antibodies used in this study were: anti-mouse CD45 (1:200, BioLegend, #157205), anti-mouse CD8 (1:100, Miltenyi Biotec, #130-177-776) and anti-mouse IFN-γ (1:200, BioLegend, #505808), anti-mouse CD11b PECy7 (1:200, BioLegend #101216), anti-mouse F4/80 APC (1:200, BioLegend, #17-4801), anti-mouse CD206 PE Dazle (1:200, BioLegend #141732) and anti Arginase1 AF488 (1:200, Thermo Fisher Scientific #53-3697-82). For intracellular staining, fixation and permeabilization were carried out using the intracellular Fix and Perm. Kit (Thermo Fisher Scientific #88-8824-00) following manufacturer's recommendation. For intranuclear staining, fixation and permeabilization were carried out using the True-Nuclear Transcription Factor Buffer Set (BioLegend, #424401) as manufacturer's protocol. All data were recorded on a BD FACS Aria III flow cytometer (BD Biosciences) and analyzed using FlowJo V.10 software for Windows (BD Biosciences).

Quantitative real-time polymerase chain reaction

The RNA was isolated using the mTDK (Miltenyi Biotec, #130-096-730) and the gentleMACS Dissociator (Miltenyi Biotec) and the cDNA was produced using the SuperScript II Reverse Transcriptase Kit (Thermo Fisher Scientific) according to the manufacturer's protocols. RT-PCR was performed at 60°C annealing temperature using primers (Thermo Fisher Scientific) listed in online supplemental table S7. Actin was used as housekeeping gene. The mRNA expression was measured using the Luna Universal qPCR Master Mix (New England Biolabs). Relative gene expressions were calculated by 2−ΔΔCt formulations.

Macrophage polarization assay in bone marrow-derived cells

Bone marrow cells collected out of the femur bones from C57Bl6/N mice were washed out with 1× PBS (Gibco, #11503387) by using an eclipse needle (BD#305892). Cells were meshed through 100 µm sterile strainers (pluriSelect #43-50100-01). For the lysis of erythrocytes, bone marrow suspension was incubated with 1× RBC Lysis Buffer (BioLegend, #420301) for 5 min and washed twice with PBS before further processing. About 6×10^6 cells were plated out into 6-well plate within 5 mL of DMEM with stable Glutamin (Bio&Sell #BS.FG0435) supplemented with 10% FCS, 100 µg/mL streptomycin (Gibco, #15140122) and 10ng/mL M-CSF (Miltenyi #130-094-129). At day 3, 2.5 mL fresh medium supplemented with M-CSF was added to the cells. The cells were harvested at day 6 by using 0.25% Trypsin (Gibco #25200056). The polarization of BMDMs was performed into 12-well plates by seeding out 0.4×10^6 cells/well and incubated for 24 hours at 37°C with 5% CO_2. M1 polarization of macrophages was done by adding 2 mL of DMEM with stable Glutamin supplemented with 10% FCS, 1% P/S and 100 ng/mL LPS (Sigma #501323). The polarization of BMDMs into M2 macrophages was performed by adding 2 mL of DMEM with stable Glutamin supplemented with 10% FBS, 1% P/S and 20 ng/mL interleukin-4 (IL-4) (Miltenyi #130-094-061). After incubation, cells were harvested by using 0.25% Trypsin and samples were generated for flow cytometry and qPCR analysis.

Steroid activity assay on polarized bone marrow-derived macrophages

Isolated BM cells were incubated as described above. On day 2, 2.5 mL M-CSF supplemented medium was added to the cells. Cells were harvested at day 5. Polarization of BMDMs was performed into 24-well plates by seeding out 25×10^5 cells per well and incubated for 48 hours at 37°C with 5% CO_2. Polarization into M1 and M2 macrophages was performed as descibed before. In addition, cells were treated with 16 µM 11-DHC (Biomol #72-23-1) and 0.1 µM 11beta-HSD1 inhibitor, 10j (Merck #385581). After incubation, cells were harvested for FACS analysis.

Immunohistochemistry

Serial sections (4 µm thickness) were prepared from FFPE tumor biopsy samples or healthy human liver. Standard hematoxylin and eosin staining was performed for tissue morphology visualization. Tumor area was marked as region of interest (ROI). Human FFPE tumor tissues were stained for 11-beta-hydroxysteroid dehydrogenase (immunohistochemistry (IHC)). Samples were deparaffinized with two 100% Xylene (AppliChem, #1317691612)

steps of 10 min followed by an ethanol dilution series of 100%, 95%, 90%, 80%, 70% and 50% 5 min each. After 5 min washing step on distilled water, samples were blocked with 3% hydrogen peroxidase (Sigma-Aldrich, #H1009) for 15 min at room temperature (RT). Washing and blocking steps were repeated for 5 min. Staining continued at the Autostainer Link 48 (Dako) with steps including hematoxylin nuclei staining, AP1 Dako Red (Dako), AB2 Dako Red (Dako), 11ß-Hydroxysteroid Dehydrogenase polyclonal antibody (Cayman Chemical, Cat#100004303) staining. Slides were digitalized using Amperio AT2 (Leica Biosystems) at the West German Biobank Essen. Human HSD11B1 expression analysis on a cell-to-cell basis was performed using the Definiens Tissue Studio Software (Definiens). Intratumoral analysis of each sample was made using the marked ROI. Individual HSD11B1 parameters were defined according to the corresponding IgG control. The 'background' intensity given by the IgG control was used as threshold. Areas without nuclei in between the tumor area (wholes, cuts, punch biopsies) were excluded in order to calculate the individual number of positive cells per total number of tumor cells.

Immunofluorescence/CODEX

Frozen murine tumor tissue sections (4 µm thickness) were fixed with Acetone (Sigma-Aldrich, #48358)/Methanol (Sigma-Aldrich, #M1775) (1:1) for 3 min on ice. After 5 min washing steps with 1× PBS (Gibco)/0.2% Tween (Sigma-Aldrich, #P1379), samples were blocked with 5% normal goat serum (NGS) (Sigma-Aldrich, #566380)/1% bovine serum albumin (Sigma-Aldrich, #A7030) for 30 min at RT. Samples were incubated overnight at 4°C with rabbit anti-mouse CD4 (BD Pharmingen, Cat #550278) or rat anti-mouse CD8 (BD Pharmingen, #553027). Fluorescently conjugated secondary antibody rabbit anti-rat Alexa Fluor 488 (Invitrogen, #A-11006) and DAPI (Sigma-Aldrich, Cat #D9542) were applied for 30 min at RT followed by 5 min washing steps. Stained slides were mounted with Fluoromount-G (SouthernBiotech, #0100-01) and stored at 4°C. Images were acquired using the AxioObserver.Z1 (Zeiss). Intratumoral quantification of $CD4^+$ and $CD8^+$ cells were quantified using ImageJ software (Fiji). A detailed description of the CO-Detection by indEXing (CODEX) tissue imaging is provided as online supplemental methods.

3′mRNA sequencing and initial processing

The 3′mRNA-seq library preparation was performed by the University Hospital Bonn (UKB) NGS core facility with the forward QuantSeq 3′mRNA-Seq Library Prep Kit for Illumina (Lexogen GmbH, #113.96) according to the manufacturer's protocol. Size distribution and library yield after the PCR step were determined by a D1000 high-sensitivity tape station (Agilent) prior to pooling of the barcoded libraries. The pooled libraries were loaded onto the Illumina HiSeq2500 platform and sequenced by a 50-cycle high-output run. Computational analysis was performed using the R-based Bioconductor computing environment. FASTQ files were aligned to the Mm10 mouse reference genome using the Rsubread aligner package.[31] To adjust the alignment procedure to 3'mRNA-seq data, the Rsubread align function was executed without trimming but allowing for mismatches in the initial cycles. Only reads with at least 45 bases in length were included in the analysis. Initial mapping using the Rsubread algorithm ('align') allowed for ambiguous mapping (max two genomic sites to allow for junction reads), but gene level summary with the 'featureCounts' methods was set to unique mapping. The 'voom' method of the limma package was used for normalization and linear modeling.[32] The mRNA expression values were transformed to log2 values of read counts per million (log2 cpm).

Gene signature and differential gene expression analyses

Gene set enrichment analysis (GSEA) was performed using a Java-based stand-alone version.[33] Gene set collections were obtained from the Molecular Signature Database (MSigDb V.7.2, https://www.gsea-msigdb.org).[34] The preranked gene list mode was used for the analyses with 1000 permutations and default settings. GSEA plots were generated with a slightly modified version of the R-function replotGSEA that can be accessed via https://github.com/PeeperLab/Rtoolbox/blob/master/R/ReplotGSEA.R. Raw sequencing data will be available through the European Nucleotide Archive (ENA) under the accession numbers PRJEB46156, PRJEB46157, PRJEB46158 and PRJEB46159.

Analysis of public scRNA-seq datasets

The scRNA-seq dataset of Jerby-Arnon *et al*[35] was downloaded from Gene Expression Omnibus (accession number GSE115978). The matrix of normalized counts (Transcript Per Kilobase Million) was used to create a Seurat object in Seurat package in R.[36] Cells having <1000 and >7500 genes expressed were filtered out and the *HSD11B1* expression was plotted across all the cell types. The scRNA-seq data set of Sade-Feldman *et al*[37] was downloaded from the Single Cell Portal (https://singlecell.broadinstitute.org/single_cell). Similarly, as the data analysis of Jerby-Arnon *et al*, the matrix of normalized counts (Transcript Per Kilobase Million) was used to create a Seurat object and cells having <1000 genes expressed filtered out. Next, the *HSD11B1* expression was plotted across all the clusters identified in this study and between responders and non-responders. A two-sided Wilcoxon signed-rank test was used to test the statistical difference of the *HSD11B1* expression between ICI responders and non-responders overall.

Statistics

Information on the study outline, sample size and statistical analysis (statistical tests) is shown in the main text and figure legends. Independent experiments are presented individually or combined, as indicated in the

figure legends. Group comparisons were statistically with Student's t-test or Wilcoxon rank-sum tests or Kruskal-Wallis test dependent on the type of input data and with a 95% CI. In case of multiple comparisons, corrections for multiple testing were done with the Benjamini and Hochberg method. Data show the mean values±SD or SEM. Statistical significance is indicated in the figures as follows: *p<0.05; **p<0.01; ***p<0.001; ****p<0.0001. P values >0.05 are not indicated.

RESULTS

Hsd11b1 expression increases early during adoptive T cell therapy of mouse melanomas

First, we asked whether there is evidence that therapy-induced T cell infiltration into melanomas promotes GC-driven negative feedback signaling. For hypothesis generation, we interrogated our previously performed experiments and dataset of B16F1 syngeneic mouse melanoma model treated with adoptive cell transfer (ACT) using Pmel-1 $CD8^+$ T cells[28] (online supplemental figure 1A). T cell receptor-transgenic Pmel-1 T cells are directed against the melanocyte differentiation antigen gp100 (also known as Pmel).[38] Comparing transcriptomes of ACT-treated vs non-treated B16F1 melanomas early during ACT, GSEA showed strong activation of interferon responses and suppression of cell proliferation (E2F targets) (online supplemental figure S1B,C and table S1). The proinflammatory TME switch caused by ACT was evidenced by increased levels of marker genes for (cytotoxic) T cells and myeloid cells as well as proinflammatory cytokines and negative immune checkpoints like PD-L1 (*Cd274*) (online supplemental figure S1D). With regard to core GC pathway genes involved in GC synthesis (eg, *Cyp11a1*), GC activation (*Hsd11b1*) and the GR receptor itself (*Nr3c1*), we found significantly increased expression of *Hsd11b1* expression in ACT-treated samples and positive trends for *Cyp11A1* and *Nr3c1* (online supplemental figure S1E). *Hsd3b7*, also significantly induced, is known to play a role and in bile acid synthesis, but a role in GC synthesis has not been reported so far.[39] Given that HSD11B1 activity critically regulates pre-receptor GC activation and GC recycling in tissues independently of local GC synthesis,[15] we focused on *Hsd11b1* expression and its potential cellular source(s). To this end, we determined the genes showing the strongest correlation with *Hsd11b1* levels in ACT-treated vs non-treated B16F1 melanomas. Intersection of the top 50 genes with the Immgen project transcriptomes of murine immune cell subtypes revealed the highest associations with myeloid immune cell subtypes such as neutrophilic granulocytes, monocytes and macrophages (online supplemental figure S1F).[40–42] In ACT-treated melanomas, increases in *Hsd11b1* level paralleled increases in immune cell signature expression, in particular myeloid cells and cytotoxic T cells (online supplemental figure S1G,H). In summary, there is evidence that *Hsd11b1* expression increased on ACT treatment in B16F1 melanomas in parallel to immune cell infiltration suggesting GC activation and recycling by HSD11B1 could be a negative feedback mechanism within the TME early during immunotherapy.

HSD11B1 expression in human melanomas and response to ICI therapy

Next, we tested the *HSD11B1* expression in a publicly available scRNA-sequencing dataset from human melanomas containing malignant, immune and stromal cells.[35 37] In line with our findings from murine melanomas, myeloid cells (macrophages) appeared as the predominant cell population expressing *HSD11B1* in human melanomas (figure 1A). Of note, in a second publicly available scRNA-sequencing dataset from human melanomas containing only immune cells from the TME,[37] the expression of *HSD11B1* was significantly higher in ICI non-responders than responders and again predominantly confined to macrophages (figure 1B,C). To corroborate this finding, we assessed the expression of HSD11B1 in human melanomas by IHC. Control stains confirmed high expression of HSD11B1 in the liver (online supplemental figure S2A). We then analyzed tissue specimens (prior to therapy) from a cohort of 24 patients with melanoma treated with ICIs (online supplemental table S2). In line with the scRNA-seq data, HSD11B1 expression was generally absent or weak in the melanoma cell compartment, whereas infiltrating immune cells stained strongly positive (figure 1D). Using automated quantification of IHC signals, we found an association between increased numbers of $HSD11B1^+$ cells and poor responses to ICI therapy in our patient cohort (figure 1E). In one additional case with PD as best clinical response, we noticed a uniform and strong signal in the melanoma cells (figure 1F). Even though scRNA-seq data provided little evidence for *HSD11B1* expression in human melanoma cells, interrogation of the Cancer Cell line Encyclopedia (CCLE) database suggested that about 10% (6/63) of melanoma cell lines express detectable or even high levels of *HSD11B1* (online supplemental figure S2B). We analyzed a small patient cohort (n=4), for which paired biopsies were available prior and under ICI therapy, for HSD11B1 expression by IHC (figure 1G). Though not statistically significant, we found a trend toward an increase of $HSD11B1^+$ cells in melanomas under ICI therapy (figure 1H). Finally, we established a CODEX tissue imaging to validate HSD11B1 expression in $CD68^+$ macrophages in patient-matched biopsies from a melanoma (Sox 10^+ melanoma cells) prior (figure 2A) and under (figure 2B) ICI therapy showing a strong recruitment of intratumoral $HSD11B1^+$ macrophages under therapeutic intervention. Thus, we had evidence for elevated HSD11B1 level in mouse and human melanomas in response to immunotherapy.

Hsd11b1 expression and activity in mouse melanoma models

Next, we aimed at investigating the functional role of HSD11B1 for ICI therapy in syngeneic mouse melanoma models. HCmel12 melanoma cells, derived from the *Hgf-Cdk4^{R24C}* melanoma mouse model,[29] showed the highest

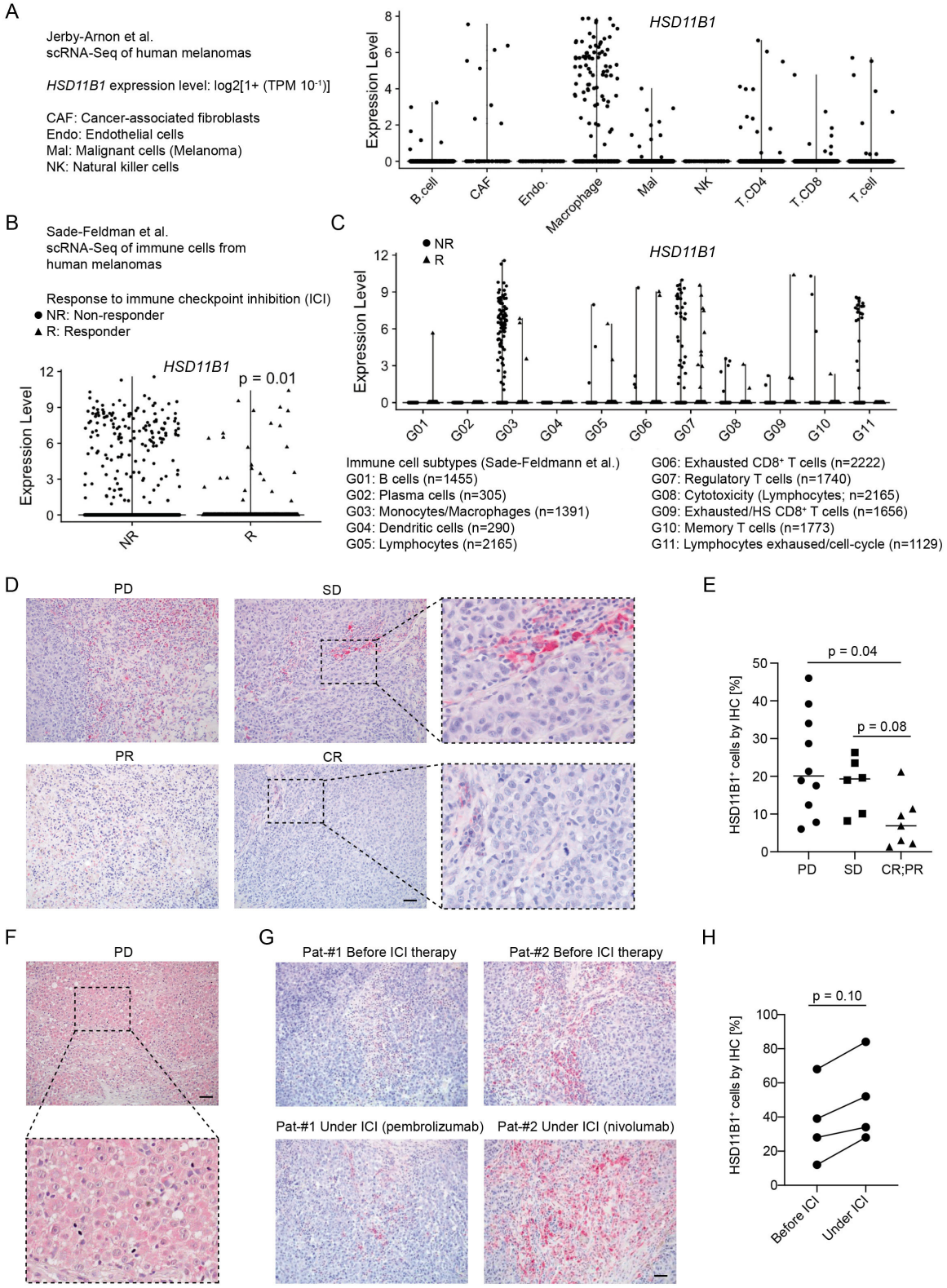

Figure 1 HSD11B1 expression in human melanomas associates with clinical response to ICI therapy. (A–C) Violin plot visualization of *HSD11B1* expression in publicly available scRNA-seq datasets from human melanomas separated by cell types (A,C) or response to ICI (B) as indicated. (D) Detection of HSD11B1 expression in human melanomas by IHC. Right panels. Zoom-in views as indicated. (E) Summary of automated quantification of HSD11B1 signals and group comparisons by best clinical responses to ICI therapy. (F) Melanoma case with strong IHC signal for HSD11B1 within melanoma cell compartment. (G) HSD11B1 expression by IHC expression in patient-matched melanoma biopsies of patients finally diagnosed for PD before and under ICI therapy. (H) Quantification of (F) by paired comparisons. Scale bars=50 µm (C, E, F). Statistics: Unpaired (B, E) and paired (H) Wilcoxon rank-sum tests. CR, complete response; ICI, immune checkpoint inhibitor; IHC, immunohistochemistry; PD, progressive disease; PR, partial response; SD, stable disease.

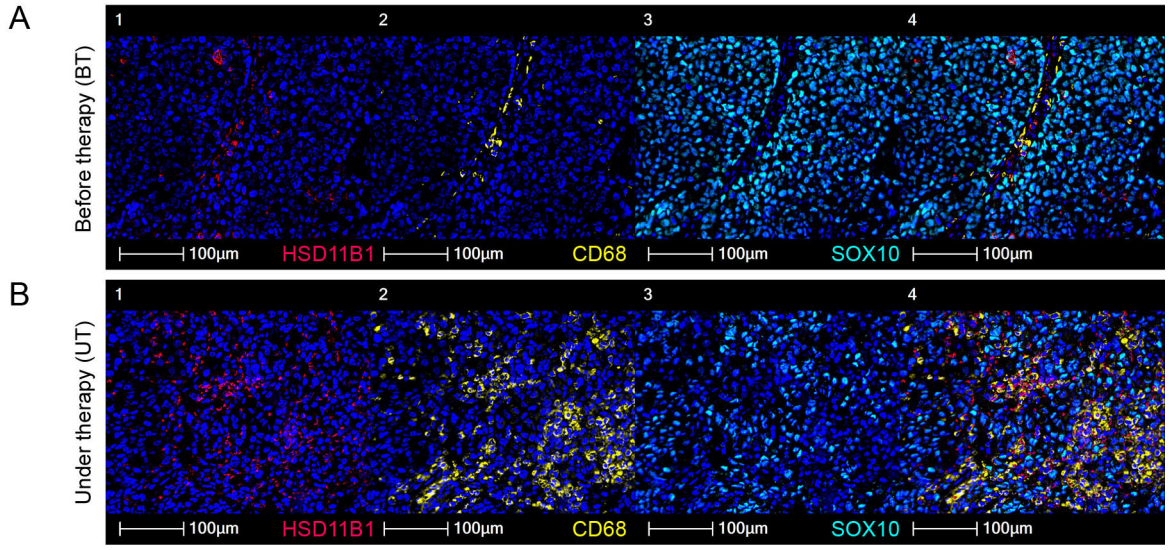

Figure 2 Recruitment of HSD11B1$^+$ macrophages in human melanoma under ICI therapy. Co-detection by indexing tissue imaging for HSD11B1 (red), CD68$^+$ macrophages (yellow), Sox 10$^+$ melanoma cells (light blue) and DAPI (nuclei, dark blue) before (A) and under ICI therapy (B). Scale bars=100 µm. ICI, immune checkpoint inhibitor.

level of *Hsd11b1* expression and CM cells the lowest (figure 3A). We established CM and LN melanoma cells from a cutaneous lesion and an LN metastasis, respectively, which had developed spontaneously in our *Mt-Ret* mouse melanoma model.[26 43] In rodents, HSD11B1 converts inactive 11-DHCS to active CS that can be easily detected by CS-specific ELISAs. To validate the assay and determine 11-DHCS to CS conversion kinetics, we generated *Hsd11b1*$^{-/-}$ variants of both HCmel12 cells (*Hsd11b1*$^{S55fs*/G57fs*}$) and CM cells (*Hsd11b1*$^{S55*/S55*}$) by CRISPR-Cas9 as well as reconstitution controls by ectopically expressing *Hsd11b1* (pRP.*Hsd11b1*) in HCmel12.*Hsd11b1*$^{-/-}$ and CM.*Hsd11b1*$^{-/-}$ cells (figure 3B). In HCmel12 cells, 11-DHCS to CS conversion was rapid and almost complete, in contrast to CM cells. All *Hsd11b1*$^{-/-}$ variants lacked 11-DHCS to CS conversion activity, which was fully restored on *Hsd11b1* re-expression. Comparing all four mouse melanoma cell lines, 11-DHCS to CS conversion correlated with differences in *Hsd11b1* expression levels (figure 3C). Given that scRNA-seq and CCLE data suggested mostly low level of *HSD11B1* expression in human melanoma cells, we considered the CM cell line with the lowest *Hsd11b1* expression and activity in our panel as the most appropriate model. The LN cell line with intermediate *Hsd11b1* expression and activity was used for comparison as it is also derived from the *Mt-Ret* melanoma mouse model.

PD-1 blockade-sensitive CM melanoma model and resistance by HSD11B1 overexpression

Both the CM and the LN models showed rapid growth after subcutaneous inoculation with matrigel into the flank of syngeneic mice. We compared the transcriptomes of non-treated CM vs LN melanomas by GSEA and found that interferon response gene sets (IFN-γ) were the most significantly enriched (figure 3D, online supplemental table S3). Of note, CM and LN cells were equally sensitive to IFN-γ in vitro (figure 3E), which argued for microenvironmental differences between CM and LN tumor in vivo. As several clinical studies associated IFN-γ pathway activity with good responses to ICI, we tested the efficacy of PD-1 blockade vs IgG control in CM and LN models. Taking into consideration the rapid growth kinetics, we decided for a priming protocol starting injections of the antibodies 1 day prior to melanoma cell inoculation. We observed that anti-PD-1 (αPD-1) significantly reduced the growth of CM melanomas but not LN melanomas when compared with IgG-treated controls (figure 3F). RNA-seq analyses also confirmed differential responsiveness to PD-1 blockade by showing downregulation of proliferation-associated genes (E2F target genes) only in CM melanomas (figure 3G). In line with our findings so far, *Hsd11b1* expression increased and correlated with cytotoxic T cell and myeloid cell content, estimated by marker gene signatures as surrogate measures, in αPD1-treated CM melanomas (figure 3H,I). Then, we wondered whether increasing HSD11B1 activity in the CM model would limit responsiveness to PD-1 blockade. Indeed, the growth of CM melanomas with ectopic expression of *Hsd11b1* (CM.pRP.*Hsd11b1*) was insensitive to αPD-1 treatment (figure 3J,K). As tumors tended to become necrotic rather rapidly, we harvested tumors at day 8 to analyze CD8$^+$ and CD4$^+$ T cell infiltration by immunofluorescence. Consistently, CM.pRP.*Hsd11b1* melanomas showed reduced CD8$^+$ and CD4$^+$ T cell infiltration under PD-1 blockade when compared with control CM melanomas (figure 3L,M). We concluded that increased HSD11B1 activity locally in the TME, modeled by enforced expression in tumor cells, limited both the efficacy of αPD-1 therapy and T cell recruitment.

HSD11B1 inhibitors improve PD-1 blockade in CM mouse melanoma model

Consequently, we asked whether pharmacological inhibition of HSD11B1 would improve αPD-1 therapy, as

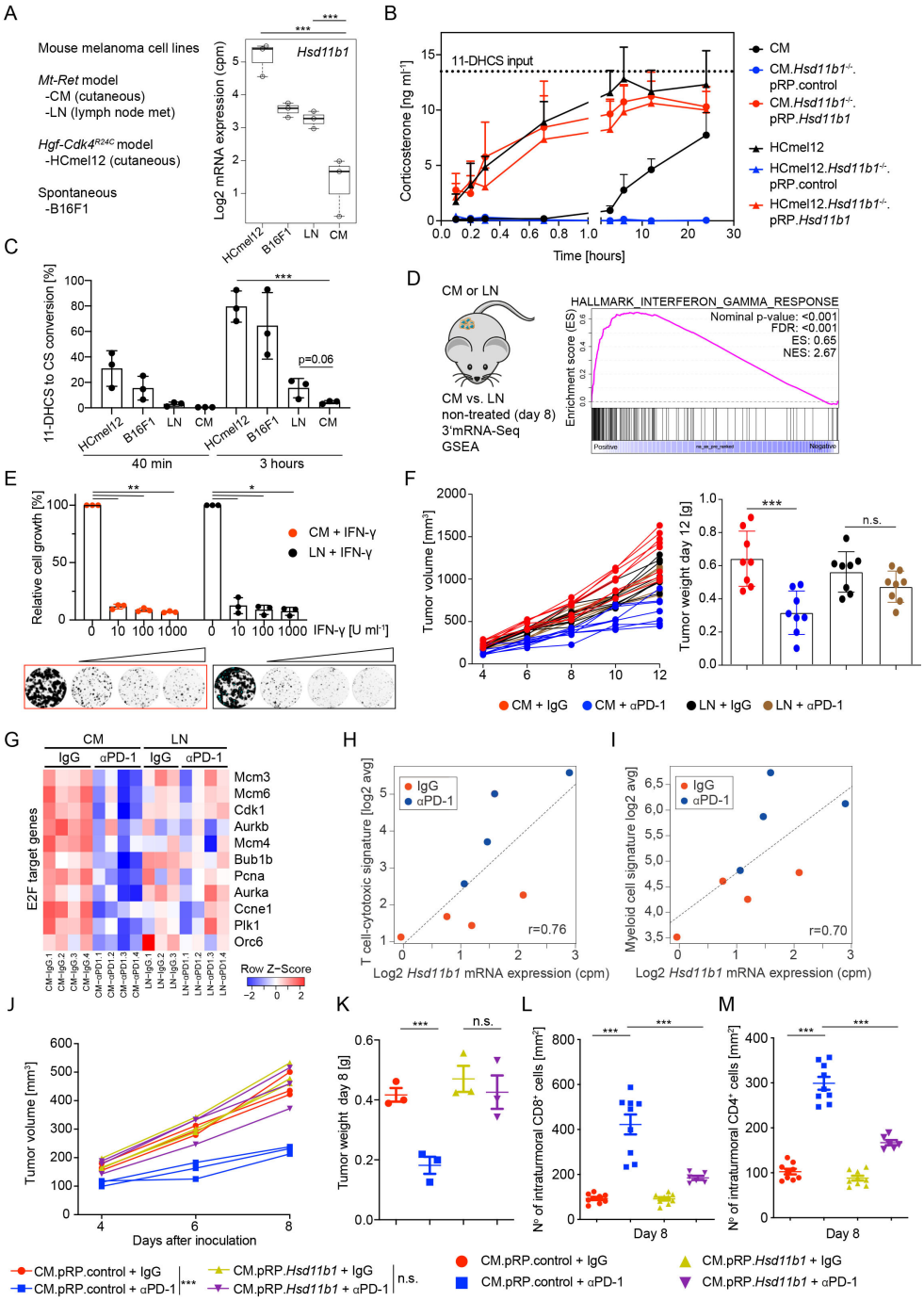

Figure 3 HSD11B1 expression confers resistance to PD-1 blockade. (A) Overview of mouse melanoma cell lines and *Hsd11b1* expression (3'mRNA-seq). (B) Kinetic of 11-DHCS to CS conversion in indicated cell lines assayed by CS-specific ELISA (n=3). Dashed line indicates input (100%) of 11-DHCS. Error bars, SD. (C) 11-DHCS to CS conversion (% of input 11-DHCS) in indicated cell lines at 40 min and 3 hours assayed by CS-specific ELISA (n=3). (D) GSEA plot for indicated gene set. Comparison of CM and LN transcriptomes (3'mRNA-seq). (E) In vitro cell growth of CM vs LN cells exposed to IFN-γ. Upper panel: Quantification of n=3. Lower panel: Representative images of stained tissue culture wells. (F) Tumor growth kinetics (left) and final tumor weight at day 12 (right) of CM and LN melanomas treated with αPD-1 or IgG control. (G) Heatmap showing proliferation-associated gene expression (3'mRNA-seq) in CM and LN melanomas from (F). (H, I) Correlation of *Hsd11b1* expression with T cell (cytotoxic) marker genes (H) and myeloid cell marker genes (I) in CM melanomas treated with αPD-1 or IgG control. (J) Individual tumor growth curves and (K) tumor weight (at day 8) of CM melanomas ectopically expressing *Hsd11b1* (pRP.*Hsd11b1*) vs CM controls (pRP) treated with αPD-1 or IgG control. (L, M) Intratumoral $CD8^+$ T cells (L) and $CD4^+$ T cells (M) assessed by immunofluorescence from multiple representative regions. Statistics: *p<0.05, **p<0.01, ***p<0.001. Two-sided unpaired t-tests (B, F, K–M), with logarithms (C, E). Correction for multiple comparison with Benjamini and Hochberg method (E). 11-DHCS, 11-dehydrocorticosterone; CM, cutaneous melanoma; CS, corticosterone; FDR, false discovery rate; GSEA, gene set enrichment analysis; IFN-γ, interferon-γ; LN, lymph node; (N)ES,(normalized) enrichment score; r, Pearson's correlation coefficient.

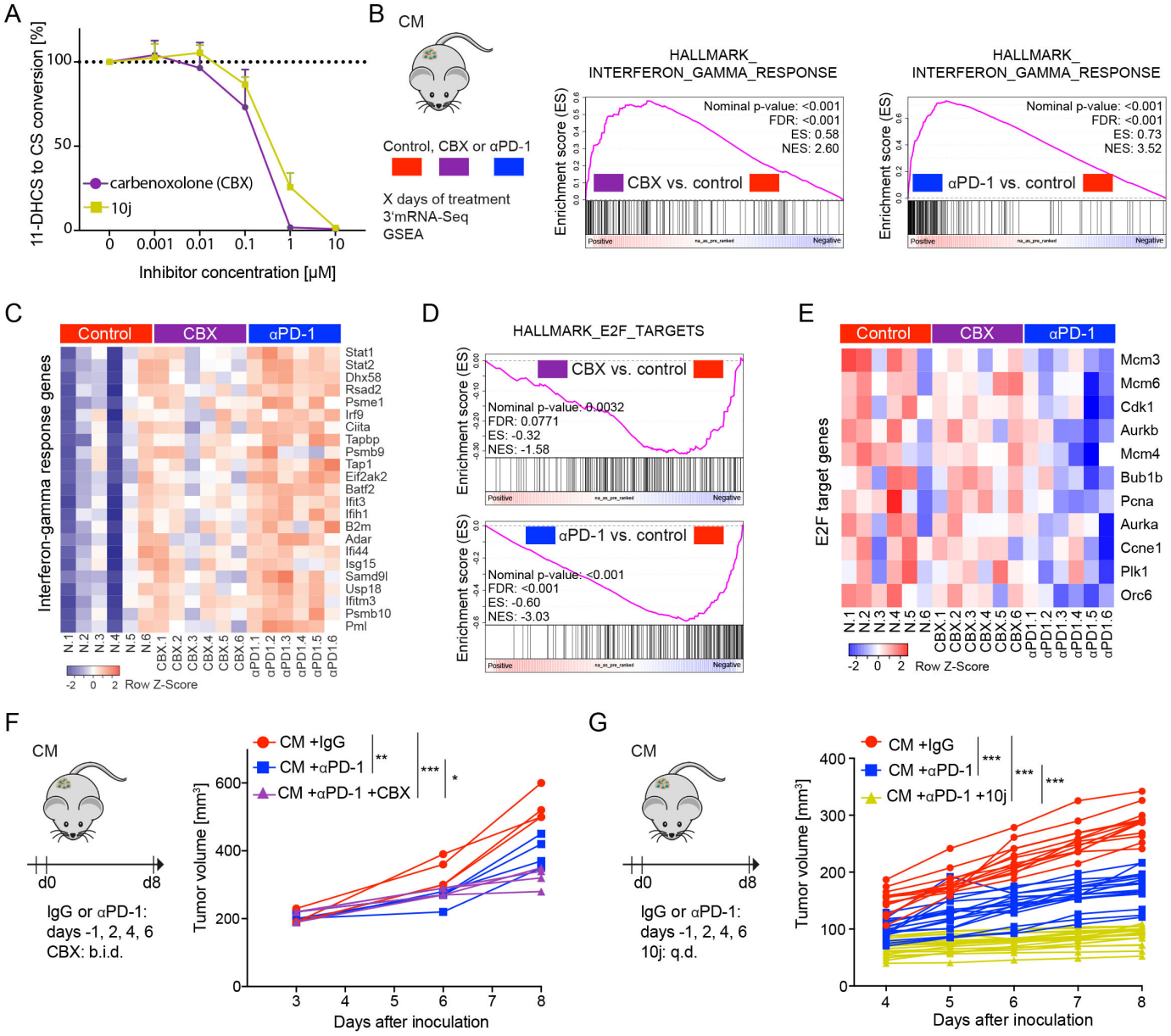

Figure 4 Pharmacological HSD11B1 inhibition enhances anti-PD-1 therapy. (A) Titration of HSD11B1 inhibitors carbenoxolone (CBX) and 10j and inhibitory effect on 11-DHCS to CS conversion (% of input 11-DHCS) assayed by CS-specific ELISA in CM cells. (B) Overview of CM melanoma samples (n=6 per group) for 3'mRNA-seq analysis and GSEA plots of top enriched interferon response gene sets in CBX and αPD-1-treated CM melanoma samples compared with non-treated controls. (C) Heatmap visualizing expression of subset of interferon response genes in CM melanoma samples from (B). (D) GSEA plots for proliferation-associated gene sets. Samples and group comparisons as in (B, C). (E) Heatmap visualizing expression of subset of proliferation-associated genes in CM melanoma samples from (B). (F) Individual CM melanoma growth curves treated as indicated (n=4 per group). (G) Individual CM melanoma growth curves treated as indicated (n=13 control group, n=17 αPD-1 and n=17 αPD-1 + 10j group). Statistics: *p<0.05, **p<0.01, ***p<0.001. Two-sided unpaired t-tests (F, G) with correction for multiple comparisons (Benjamini and Hochberg method). 11-DHCS, 11-dehydrocorticosterone; CM, cutaneous melanoma; CS, corticosterone; FDR, false discovery rate; GSEA, gene set enrichment analysis; (N)ES, (normalized) enrichment score.

HSD11B1 inhibitors have been in the focus of drug design for several years for metabolic disorders.[15 44] CBX and the 11beta-HSD1 inhibitor, 10j are two well-characterized HSD11B1 inhibitors used for experimental in vivo studies,[45–47] whereby CBX is considered as a non-selective HSD11B1 inhibitor. Using CM cells pretreated with DMSO, CBX or 10j prior 11-DHCS incubation, we confirmed that both inhibitors blocked 11-DHCS to CS conversion with comparable efficacies (figure 4A). Then, we treated CM melanoma-bearing mice with CBX, αPD-1 or left them untreated as controls and generated transcriptome data by RNA-seq. GSEA showed that CBX treatment also led to an increase of interferon pathway activity, although to a lesser extent than PD-1 blockade (figure 4B,C, online supplemental table S4A,B). Proliferation-associated gene sets (E2F targets) were moderately reduced in

CBX-treated CM melanomas when compared with αPD-1 treatment (figure 4D,E, online supplemental table S4C,D). Following the initial molecular characterization of HSD11B1 inhibition, we next combined PD-1 blockade with CBX and observed improved tumor growth control of CM melanomas (figure 4F). Similar results were obtained when we combined PD-1 blockade with 10j (figure 4G). We concluded that pharmacological HSD11B1 inhibition improved the efficacy of PD-1 blockade in our CM melanoma model.

HSD11B1 inhibition drives a proinflammatory signature in tumor-associated macrophages

Because expression of HSD11B1 has been described predominantly in macrophages, we wondered whether expression was dependent on macrophage polarization and/or occurred in the context of tumor presence. First, macrophage colony-stimulating factor (M-CSF)-driven differentiation of bone marrow-derived cells from tumor-bearing mice, with or without therapeutic intervention, into macrophages (figure 5A) followed by lipopolysaccharide (LPS)-induced or IL-4-induced polarization into Ly6C$^+$arginase1$^-$CD206$^-$ M1 or Ly6C$^-$arginase1$^+$CD206$^+$ M2 (figure 5B) did not result in significant differences in HSD11B1 expression (figure 5C,D). However, we observed a slight, although non-significant, trend toward lower HSD11B1 expression in CD11b$^+$F4/80$^+$ macrophages isolated from CM-transplanted tumors co-treated with αPD-1 and 10j (figure 5E,F). Interestingly, as presented in figure 5G, 10j treatment under PD1 blockage supports the anti-tumoral phenotype of TAMs by decreasing their CD206 and arginase-1 expression (figure 5G). In addition, we found an upregulation of the proinflammatory molecule IL-12 in TAMs under dual therapy (figure 5H). Macrophage-derived IL-12 has previously been shown to trigger potent IFN-y secretion in T cells. Thus, we conclude that 10j promotes their ability of TAMs to activate T cells in regulating IFN-y secretion in these cells.

HSD11B1 inhibition promotes IFN-γ production by CD8$^+$ T cells under PD-1 blockade

As shown above, CM melanoma cells were highly sensitive to IFN-γ exposure in vitro and GCs are known to impair cytotoxic cytokine production by T cells including IFN-γ. Therefore, we asked whether HSD11B1 inhibition promoted IFN-γ by intratumoral CD8$^+$ T cells. After co-therapy with αPD-1 and 10j, we observe a significant upregulation of IFN-γ-dependent immunity suggesting a positive immunostimulatory effect triggered by the combination therapy. Indeed, flow cytometric analyses showed highest frequencies of IFN-γ $^+$CD8$^+$ T cells in CM melanomas of mice treated with αPD-1+10j when compared with the other treatment conditions (figure 6A–C). Detailed analyses of CD8$^+$ T cells isolated from the individual treatment groups presented a significant upregulation of selected transcription factors mediating a direct positive feed-forward regulation of IFN-γ production and mediate cellular responses to IFN-γ (online supplemental figure S4).

To confirm the observed effect of HSD11B1 inhibition on CD8$^+$ T cells in vitro, we devised a simplified experimental approach and exposed gp100 peptide-activated Pmel-1 CD8$^+$ T cells endogenously expressing *Hsd11b1* to 11-DHCS. Consistently, we detected reduced IFN-γ $^+$ production, which could be restored by concomitant treatment with HSD11B1 inhibitors (figure 6D–F). Finally, to assess the contribution of CD8$^+$ T cells in the CM melanoma model, we depleted CD8$^+$ T cells with antibodies and verified effective reduction of CD8$^+$ T cell frequencies in CM melanomas and tumor-draining LN by flow cytometry (figures 6G and 5H). Of note, αPD-1 monotherapy was only moderately impaired by the depletion of CD8$^+$ T cells at early time points of tumor development but was severely affected in established tumors (online supplemental figure S3). In line with our hypothesis, we found that combined treatment with αPD-1+10j was largely ineffective in mice depleted of CD8$^+$ T cells (figure 6I–K). This suggested that inhibition of GC activation by HSD11B1 elicited both anti-tumor and pro-tumor effects dependent on the presence of CD8$^+$ T cells. Thus, we propose that HSD11B1 inhibitors could be evaluated to augment T cell-initiated IFN-γ signaling in the context of ICI therapy, but only in cases with baseline CD8$^+$ T cell infiltration.

DISCUSSION

Systemic levels of GCs are regulated by the hypothalamic–pituitary–adrenal axis,[14] but mouse models with conditional deletion of *Hsd11b1* in adipocytes or hepatic myofibroblasts showed that local regulation of GC activity is important for metabolism and tissue regeneration.[16 48] Furthermore, the majority of circulating GCs are bound to cortisol-binding globulin (CBG) and thus inactive, but can be deliberated by cleavage of CBG through neutrophil elastase at sites of inflammation.[49] Now, using syngeneic mouse models of melanoma, our study identified local GC activation by HSD11B1 as a druggable negative feedback mechanism of anti-tumor immune responses induced by T cell therapies.

Recent work by Grasso *et al*[8] underscored the important association between high IFN-γ signaling activity and benefit from ICI therapy by transcriptome analyses of pre-treatment and on-treatment biopsies from patients with melanoma. In view of these clinical data, our CM and LN syngeneic melanoma models, both derived from spontaneous melanomas in *Mt-Ret* transgenic mice, are of interest, as higher IFN-γ pathway activity in CM melanomas correlated with sensitivity to PD-1 blockade. Co-treatment with HSD11B1 inhibitors promoted cellular IFN-γ response and production by CD8$^+$ T cells, in line with the known immunosuppressive functions of GCs,[14] further augmenting IFN-γ signaling. In melanoma cells, IFN-γ enforces antigen presentation, release of T cell attracting chemokines (eg, CXCL9, CXCL10) and growth arrest,[8]

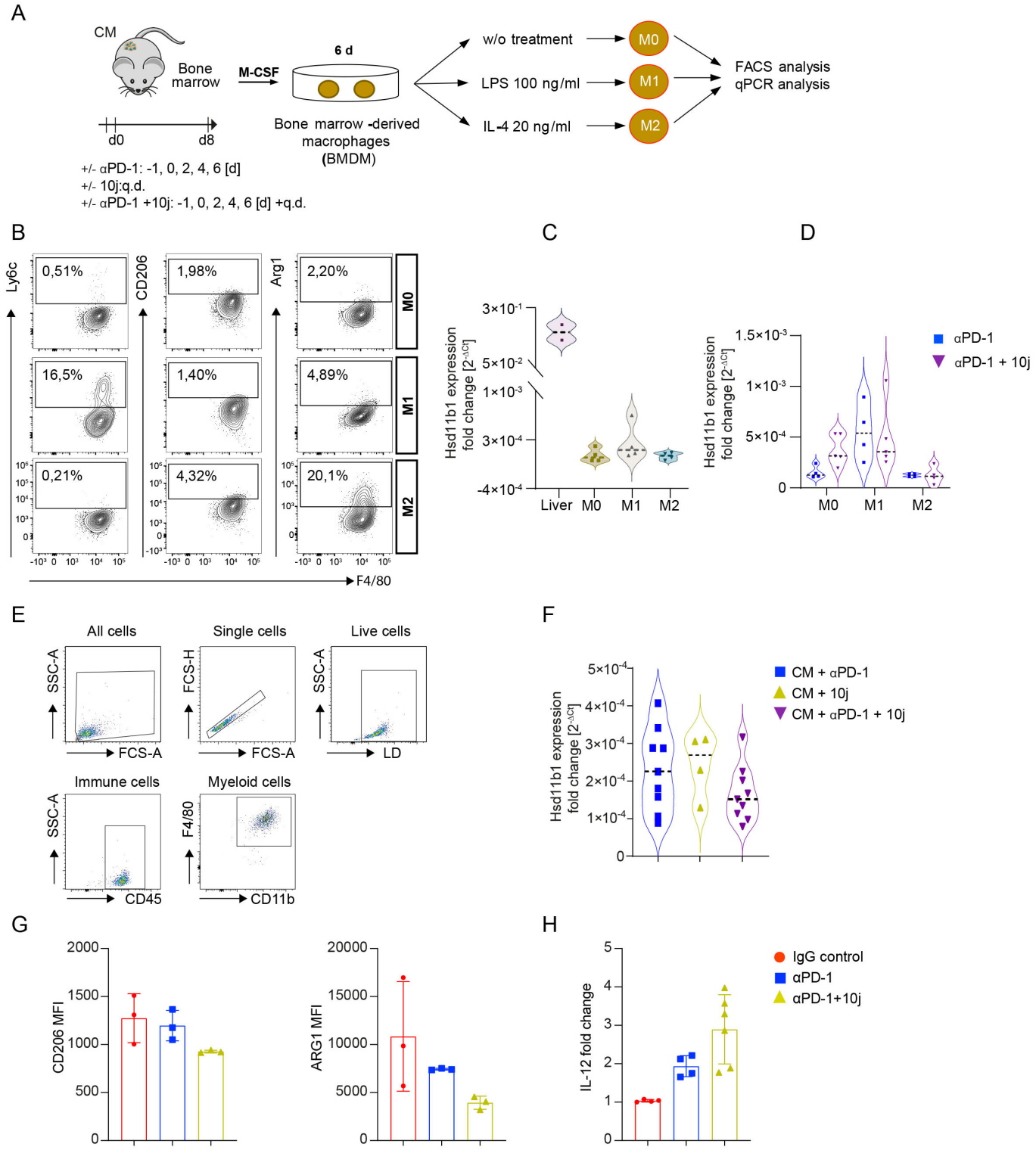

Figure 5 HSD11B1 inhibition modulates macrophage polarization and activity. (A) Experimental outline of bone marrow-derived macrophages (BMDM) and treatment conditions for in vitro polarization. (B) Representative FACS blots of Ly6C as marker for M1 and CD206 and Arg1 as markers for M2 macrophages from bone marrow-derived ($CD11b^{+}F4/80^{+}$) cells. Distribution of Hsd11b1 expression in BMDM from non-treated (C) and treated mice (D) bearing CM melanomas (n=2). Liver tissue was used as a control. Dotted line indicates the median. M0 median: 0.00005, M1 median: 0.0002, M2 median: 0.00008. (E) Sorting of tumor-derived macrophages. Gating strategy for flow cytometry. (F) Hsd11b1 expression in tumor-derived macrophages from mice bearing CM melanomas under indicated treatment conditions (n=2). (G) Detection of M2 macrophage markers CD206 and Arg1 in TAMs of mice under therapy. Median fluorescence intensity (MFI). (H) Quantitative analyses of IL-12 in tumor-derived macrophages in mice of indicated treatment conditions (n=2). CM, cutaneous melanoma; H, IL-4, interleukin-4; M-CSF, macrophage colony-stimulating factor; LPS, lipopolysaccharide; TAMs, tumor-associated macrophages.FCS, forward scatter; SSC, side scatter.

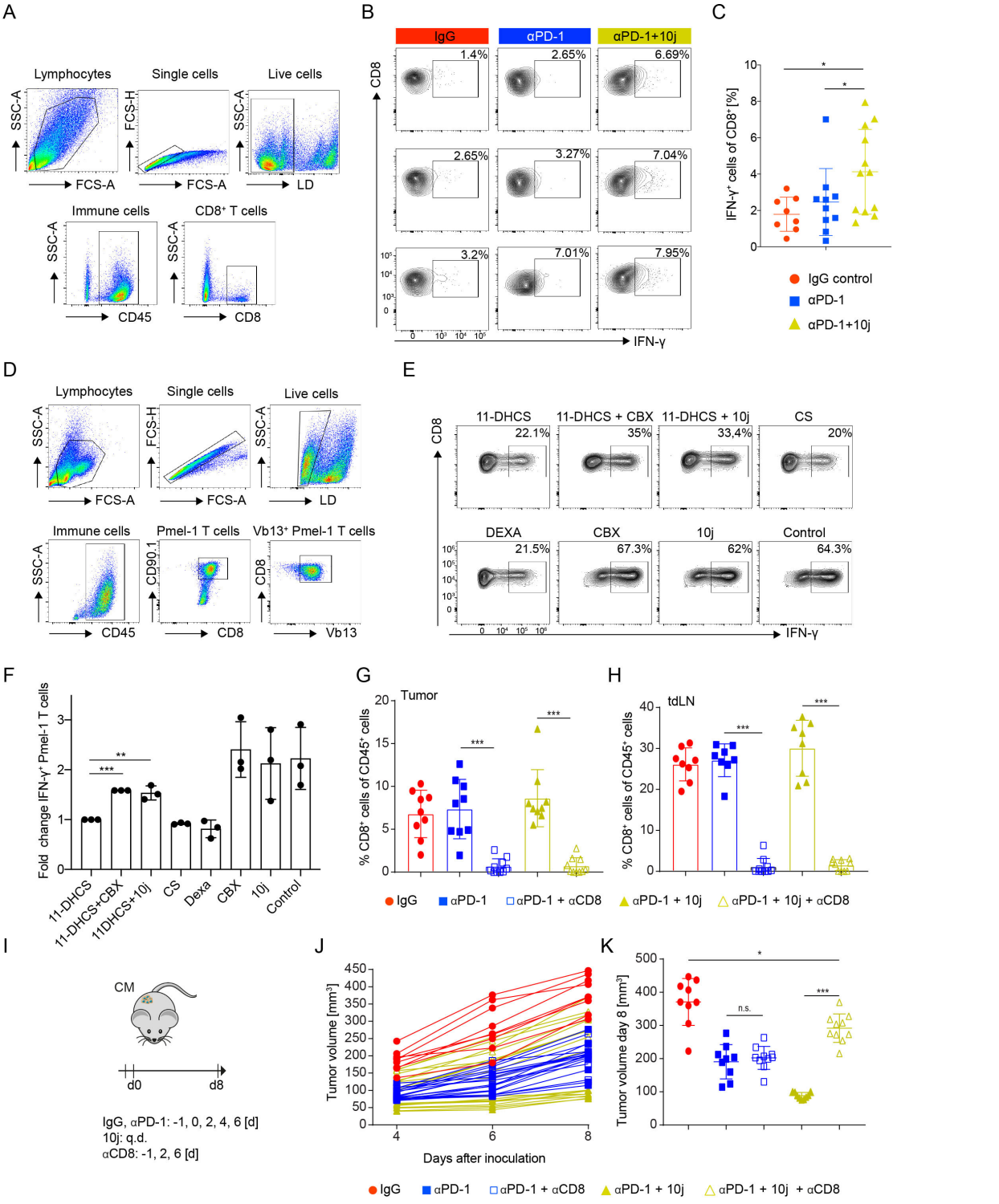

Figure 6 HSD11B1 inhibition augments IFN-γ production of CD8⁺ T cells under PD-1 blockade. (A) Effect of HSD11B1 inhibition on IFN-γ production by intratumoral (CM) CD8⁺ T cells. Gating strategy for flow cytometry. (B) Representative FACS blots showing frequencies of IFN-γ ⁺CD8⁺ cells in CM melanomas treated as indicated. (C) Quantification of experiment described in (B). Two-sided unpaired t-test with logarithms. (D) Effect of HSD11B1 inhibition on IFN-γ production by Pmel-1 T cells in vitro. Gating strategy for flow cytometry. (E) Representative FACS blots (IFN-γ positivity) of gp100 activated Pmel-1 T cells treated as indicated. (F) Quantification of experiments (n=3) described in (D, E). 11-DHCS, DEXA (100 nM), CBX and 10j (10 µM). (G) Experimental outline of CD8⁺ T cell depletion in mice bearing CM melanomas and treatment conditions. (H, I) Frequencies of CD8⁺ T cells in (H) tumor and (I) tumor-draining LN assessed by flow cytometry. (J) Individual CM melanoma tumor growth curves and (K) tumor volume at day 8 after inoculation treated as indicated with or without antibody-mediated depletion of CD8⁺ cells. Statistics: *p<0.05, **p<0.01, ***p<0.001. Two-sided unpaired t-tests (for ratios with logarithms). 11-DHCS, 11-dehydrocorticosterone; CM, cutaneous melanoma; DEXA, dexamethasone; IFN-γ, interferon-γ; tdLN, tumor-draining lymph node.

which provides an explanation why inactivating mutations of IFN-γ pathway components like *JAK2* emerge in some melanomas acquiring resistance to immunotherapy.[50–52] On the contrary, persistent interferon signaling was shown to activate an intrinsic resistance program to ICI therapy.[53] Thus, timing and duration of HSD11B1 inhibitor treatment will be critical parameters because IFN-γ can have opposing effects.

Recently, work by others also focused on the emerging role of GCs in the TME and their capability to restrain anti-tumor immunity.[18 19 25] Increased GC receptor expression and GC pathway activity were found in dysfunctional tumor-infiltrating CD8$^+$ T cells.[18] Monocyte–macrophage lineage cells were identified as main cellular source of de novo GC biosynthesis with CYP11A1 as rate-limiting enzyme, which was supported by cell lineage-specific conditional deletion of *Cyp11a1* in *LysM-Cre;Cyp11a1$^{fl/fl}$* mice. Using a similar approach, Mahata *et al*[19] showed that ablation of *Cyp11a1* in T cells using *Cd4-Cre;Cyp11a1$^{fl/fl}$* mice promoted anti-tumor immunity. Another study found evidence for GC activation by HSD11B1 but not GC synthesis in peripheral T cells,[54] suggesting that tumor-infiltrating T cells can acquire GC synthesis competency. Work by Yang *et al*[25] found a critical role for GC-induced expression of *Tsc22d3* in DCs, which impaired the capability of DCs to coordinate an effective anti-tumor immune response. In line with our findings, these recent studies emphasized the importance of local GC signaling for tumor immune surveillance. Now, our work defined GC activation by increased HSD11B1 activity in melanomas as an early event in response to ICI therapy that controls IFN-γ signaling in the TME driven by CD8$^+$ T cells. Of note, small molecule inhibitors of HSD11B1 are being developed and evaluated for the treatment of metabolic diseases including diabetes and obesity,[15 44 55] for which reason combining HSD11B1 inhibitors with ICI could be feasible drug repurposing strategy to improve cancer immunotherapy.

Immune-related adverse advents (irAEs) are well-documented side effects of ICIs and irAEs can be severe (grade 3, 4 or 5) leading to discontinuation of the treatment.[56 57] As GCs are commonly used to treat severe irAEs, there is the potential caveat that blocking GC synthesis or GC activation in combination with ICIs could aggravate irAEs or increase the likelihood of occurrence. In particular, HSD11B1 inhibition may aggravate the critical side effects of adoptive cell therapies like cytokine release syndrome. Taking these issues into consideration, a possibility is that HSD11B1 inhibitors are administered only for limited period of time to reduce the risk of ICI-related irAEs, but this is speculative. Therefore, more insights are needed how local GC regeneration by HSD11B1 influences the frequency and severity of irAEs. Our results also indicate that HSD11B1 inhibitor co-treatment with ICIs is ineffective or even pro-tumoral in the absence of CD8$^+$ T cells. For example, genetic ablation of *Hsd11b1* in macrophages was shown to promote inflammatory angiogenesis in mouse models of arthritis.[42] Thus, these issues need to be addressed faithfully before evaluating HSD11B1 inhibitors in patients with melanoma treated with ICIs.

Author affiliations
[1]Skin Cancer Unit of the Dermatology Department, Medical Faculty, West German Cancer Center, University Duisburg-Essen, Essen, Germany
[2]German Cancer Consortium (DKTK), Partner Site Essen/Düsseldorf, Essen, Germany
[3]Department of Dermatology and Allergy, University Hospital, Ludwig Maximilian University (LMU) Munich, Munich, Germany
[4]German Cancer Consortium (DKTK), Partner Site Munich, Munich, Germany
[5]Institute of Experimental Oncology (IEO), Medical Faculty, University Hospital Bonn, University of Bonn, Bonn, Germany
[6]Department of Otorhinolaryngology, University Hospital Essen, University Duisburg-Essen, Essen, Germany
[7]Institute for Experimental Immunology and Imaging, University Hospital, University Duisburg-Essen, Essen, Germany
[8]Institute of Cell Biology (Cancer Research), University Hospital Essen, University of Duisburg-Essen, Essen, Germany
[9]Department of Pediatrics III, University Children's Hospital Essen, University Duisburg-Essen, Essen, Germany
[10]Drug Discovery Hub Dortmund (DDHD) am Zentrum für integrierte Wirkstoffforschung (ZIW), Dortmund, Belgium
[11]Faculty of Chemistry and Chemical Biology, TU Dortmund University, Dortmund, Germany
[12]Center for Cancer Biology, VIB-KU Leuven, Leuven, Belgium
[13]Department of Oncology, KU Leuven, Leuven, Belgium

Twitter Jadwiga Jablonska @JablonskaLab

Acknowledgements We thank the UKB NGS core facility for help with RNA-seq experiments and the Imaging Center Essen (IMCES) for continuous support of our flow cytometry experiments.

Contributors MH and IH conceptualized, coordinated and directed the project. LMNM, DH-R, DH, SLöffek, IÖ, RT, JK, SLeonardelli, I-VW, YA-M, SE-R, AB, MB, ME and NG performed experiments and analyzed data. RT and SLeonardelli established and performed CODEX. FW provided expertise and support with macrophage differentiation and polarization analyses. IÖ and JJ performed experiments and analyzed data on TAMs and INF-γ response in T cells. DH, JP, FR, SE-R, ME, NG and MH generated statistical and RNA sequencing analysis. HH provided NGS mice used in the project. NU and DR provided expertise and support with inhibitor characterization. AS, EH and DS provided clinical material and patient information and designed the selection of the patient cohort. LMNM, DH-R, DH, SLöffek, NG, JJ, MH and IH wrote the manuscript. Manuscript review and approval was performed by all authors. IH is acting as guarantor.

Funding This work was supported in part by the Deutsche Krebshilfe (German Cancer Aid, DKH no 70113192 to IH and no 70113168 to MH), Deutsche Forschungsgemeinschaft (KFO 337: DFG/ HE 5294/2-1 no 405344257 to IH, DFG/ SCHA 422/17-1 to DS; DFG/JA-2461/7-1 and CRC TRR332 project A05 to JJ), DFG under Germany's Excellence Strategy–EXC2151-390873048 to MH and Hiege Stiftung–Die Deutsche Hautkrebsstiftung (to IH).

Competing interests None declared.

Patient consent for publication Consent obtained directly from patient(s).

Ethics approval Informed patient consent was obtained from all patients. The study was performed with approval by the ethics committee of the Medical Faculty, University Duisburg-Essen (ethics approval no 11-4715 and no 17-7708-BO). Animal experiments were performed under specific pathogen-free conditions at the Central Animal Facility of the University Hospital Bonn (Germany), Central Animal Facility of the University Hospital Essen and conducted according to the institutional and national guidelines for the care and use of laboratory animals with approval by the local government authorities (Bonn: Az: 84-02.04.2014.A128; Essen: Az: 81-02.04.2018.A184, Az: 84-02.04.2016.A480, LANUV, NRW, Munich: ROB-55.2-2532.Vet_02-22-73, Germany).

Provenance and peer review Not commissioned; externally peer reviewed.

Data availability statement Data are available upon reasonable request. All data relevant to the study are included in the article or uploaded as online supplemental information.

ORCID iDs
Irem Oezel http://orcid.org/0000-0002-7007-9928
Jadwiga Jablonska http://orcid.org/0000-0003-1490-2542
Michael Hölzel http://orcid.org/0000-0003-4048-8824
Iris Helfrich http://orcid.org/0000-0001-6150-9570

REFERENCES

1 Larkin J, Chiarion-Sileni V, Gonzalez R, *et al*. Five-Year survival with combined nivolumab and ipilimumab in advanced melanoma. *N Engl J Med* 2019;381:1535–46.
2 Robert C, Ribas A, Schachter J, *et al*. Pembrolizumab versus ipilimumab in advanced melanoma (KEYNOTE-006): post-hoc 5-year results from an open-label, multicentre, randomised, controlled, phase 3 study. *Lancet Oncol* 2019;20:1239–51.
3 Schadendorf D, van Akkooi ACJ, Berking C, *et al*. Melanoma. *Lancet* 2018;392:971–84.
4 Fritz JM, Lenardo MJ. Development of immune checkpoint therapy for cancer. *J Exp Med* 2019;216:1244–54.
5 Gide TN, Wilmott JS, Scolyer RA, *et al*. Primary and acquired resistance to immune checkpoint inhibitors in metastatic melanoma. *Clin Cancer Res* 2018;24:1260–70.
6 Kalbasi A, Ribas A. Tumour-intrinsic resistance to immune checkpoint blockade. *Nat Rev Immunol* 2020;20:25–39.
7 Sharma P, Hu-Lieskovan S, Wargo JA, *et al*. Primary, adaptive, and acquired resistance to cancer immunotherapy. *Cell* 2017;168:707–23.
8 Grasso CS, Tsoi J, Onyshchenko M, *et al*. Conserved interferon-γ signaling drives clinical response to immune checkpoint blockade therapy in melanoma. *Cancer Cell* 2020;38:500–15.
9 Liu D, Schilling B, Liu D, *et al*. Integrative molecular and clinical modeling of clinical outcomes to PD1 blockade in patients with metastatic melanoma. *Nat Med* 2019;25:1916–27.
10 Chen DS, Mellman I. Oncology meets immunology: the cancer-immunity cycle. *Immunity* 2013;39:1–10.
11 Eggermont AMM, Kicinski M, Blank CU, *et al*. Association between immune-related adverse events and recurrence-free survival among patients with stage III melanoma randomized to receive pembrolizumab or placebo: a secondary analysis of a randomized clinical trial. *JAMA Oncol* 2020;6:519–27.
12 Michot JM, Bigenwald C, Champiat S, *et al*. Immune-related adverse events with immune checkpoint blockade: a comprehensive review. *Eur J Cancer* 2016;54:139–48.
13 Okoye IS, Xu L, Walker J, *et al*. The glucocorticoids prednisone and dexamethasone differentially modulate T cell function in response to anti-PD-1 and anti-CTLA-4 immune checkpoint blockade. *Cancer Immunol Immunother* 2020;69:1423–36.
14 Cain DW, Cidlowski JA. Immune regulation by glucocorticoids. *Nat Rev Immunol* 2017;17:233–47.
15 Gathercole LL, Lavery GG, Morgan SA, *et al*. 11B-Hydroxysteroid dehydrogenase 1: translational and therapeutic aspects. *Endocr Rev* 2013;34:525–55.
16 Morgan SA, McCabe EL, Gathercole LL, *et al*. 11B-Hsd1 is the major regulator of the tissue-specific effects of circulating glucocorticoid excess. *Proc Natl Acad Sci U S A* 2014;111:E2482–91.
17 Morton NM, Holmes MC, Fiévet C, *et al*. Improved lipid and lipoprotein profile, hepatic insulin sensitivity, and glucose tolerance in 11beta-hydroxysteroid dehydrogenase type 1 null mice. *J Biol Chem* 2001;276:41293–300.
18 Acharya N, Madi A, Zhang H, *et al*. Endogenous glucocorticoid signaling regulates CD8+ T cell differentiation and development of dysfunction in the tumor microenvironment. *Immunity* 2020;53:658–71.
19 Mahata B, Pramanik J, van der Weyden L, *et al*. Tumors induce de novo steroid biosynthesis in T cells to evade immunity. *Nat Commun* 2020;11:3588.
20 John S, Sabo PJ, Thurman RE, *et al*. Chromatin accessibility pre-determines glucocorticoid receptor binding patterns. *Nat Genet* 2011;43:264–8.
21 Surjit M, Ganti KP, Mukherji A, *et al*. Widespread negative response elements mediate direct repression by agonist-liganded glucocorticoid receptor. *Cell* 2011;145:224–41.
22 Shimba A, Ikuta K. Control of immunity by glucocorticoids in health and disease. *Semin Immunopathol* 2020;42:669–80.
23 Taves MD, Ashwell JD. Glucocorticoids in T cell development, differentiation and function. *Nat Rev Immunol* 2021;21:233–43.
24 Szatmari I, Nagy L. Nuclear receptor signalling in dendritic cells connects lipids, the genome and immune function. *EMBO J* 2008;27:2353–62.
25 Yang H, Xia L, Chen J, *et al*. Stress-glucocorticoid-TSC22D3 axis compromises therapy-induced antitumor immunity. *Nat Med* 2019;25:1428–41.
26 Helfrich I, Ullrich N, Zigrino P, *et al*. Primary tumor versus metastasis: new experimental models for studies on cancer cell homing and metastasis in melanoma. *Pigment Cell Melanoma Res* 2014;27:309–16.
27 Effern M, Glodde N, Braun M, *et al*. Adoptive T cell therapy targeting different gene products reveals diverse and context-dependent immune evasion in melanoma. *Immunity* 2020;53:564–80.
28 Glodde N, Bald T, van den Boorn-Konijnenberg D, *et al*. Reactive neutrophil responses dependent on the receptor tyrosine kinase c-met limit cancer immunotherapy. *Immunity* 2017;47:789–802.
29 Bald T, Quast T, Landsberg J, *et al*. Ultraviolet-radiation-induced inflammation promotes angiotropism and metastasis in melanoma. *Nature* 2014;507:109–13.
30 Schmid-Burgk JL, Höning K, Ebert TS, *et al*. CRISPaint allows modular base-specific gene tagging using a ligase-4-dependent mechanism. *Nat Commun* 2016;7:12338.
31 Liao Y, Smyth GK, Shi W. The R package rsubread is easier, faster, cheaper and better for alignment and quantification of RNA sequencing reads. *Nucleic Acids Res* 2019;47:e47.
32 Law CW, Chen Y, Shi W, *et al*. Voom: precision weights unlock linear model analysis tools for RNA-seq read counts. *Genome Biol* 2014;15:R29.
33 Subramanian A, Tamayo P, Mootha VK, *et al*. Gene set enrichment analysis: A knowledge-based approach for interpreting genome-wide expression profiles. *Proc Natl Acad Sci U S A* 2005;102:15545–50.
34 Liberzon A, Birger C, Thorvaldsdóttir H, *et al*. The molecular signatures database (msigdb) hallmark gene set collection. *Cell Syst* 2015;1:417–25.
35 Jerby-Arnon L, Shah P, Cuoco MS, *et al*. A cancer cell program promotes T cell exclusion and resistance to checkpoint blockade. *Cell* 2018;175:984–97.
36 Satija R, Farrell JA, Gennert D, *et al*. Spatial reconstruction of single-cell gene expression data. *Nat Biotechnol* 2015;33:495–502.
37 Sade-Feldman M, Yizhak K, Bjorgaard SL, *et al*. Defining T cell states associated with response to checkpoint immunotherapy in melanoma. *Cell* 2018;175:998–1013.
38 Overwijk WW, Tsung A, Irvine KR, *et al*. Gp100/pmel 17 is a murine tumor rejection antigen: induction of self-reactive, tumoricidal T cells using high-affinity, altered peptide ligand. *J Exp Med* 1998;188:277–86.
39 Schwarz M, Wright AC, Davis DL, *et al*. The bile acid synthetic gene 3beta-hydroxy-delta (5) -C (27) -steroid oxidoreductase is mutated in progressive intrahepatic cholestasis. *J Clin Invest* 2000;106:1175–84.
40 Coutinho AE, Kipari TMJ, Zhang Z, *et al*. 11B-Hydroxysteroid dehydrogenase type 1 is expressed in neutrophils and restrains an inflammatory response in male mice. *Endocrinology* 2016;157:2928–36.
41 Heng TSP, Painter MW. Immunological genome project consortium. The immunological genome project: networks of gene expression in immune cells. *Nat Immunol* 2008;9:1091–4.
42 Zhang Z, Coutinho AE, Man TY, *et al*. Macrophage 11β-HSD-1 deficiency promotes inflammatory angiogenesis. *J Endocrinol* 2017;234:291–9.
43 Hansen W, Hutzler M, Abel S, *et al*. Neuropilin 1 deficiency on CD4+Foxp3+ regulatory T cells impairs mouse melanoma growth. *J Exp Med* 2012;209:2001–16.
44 Scott JS, Goldberg FW, Turnbull AV. Medicinal chemistry of inhibitors of 11β-hydroxysteroid dehydrogenase type 1 (11β-HSD1). *J Med Chem* 2014;57:4466–86.

45 Andrews RC, Rooyackers O, Walker BR. Effects of the 11 beta-hydroxysteroid dehydrogenase inhibitor carbenoxolone on insulin sensitivity in men with type 2 diabetes. *J Clin Endocrinol Metab* 2003;88:285–91.
46 Terao M, Tani M, Itoi S, *et al*. 11B-Hydroxysteroid dehydrogenase 1 specific inhibitor increased dermal collagen content and promotes fibroblast proliferation. *PLoS One* 2014;9:e93051.
47 Tice CM, Zhao W, Xu Z, *et al*. Spirocyclic ureas: orally bioavailable 11 beta-HSD1 inhibitors identified by computer-aided drug design. *Bioorg Med Chem Lett* 2010;20:881–6.
48 Zou X, Ramachandran P, Kendall TJ, *et al*. 11Beta-Hydroxysteroid dehydrogenase-1 deficiency or inhibition enhances hepatic myofibroblast activation in murine liver fibrosis. *Hepatology* 2018;67:2167–81.
49 Pemberton PA, Stein PE, Pepys MB, *et al*. Hormone binding globulins undergo serpin conformational change in inflammation. *Nature* 1988;336:257–8.
50 Horn S, Leonardelli S, Sucker A, *et al*. Tumor CDKN2A-associated JAK2 loss and susceptibility to immunotherapy resistance. *J Natl Cancer Inst* 2018;110:677–81.
51 Shin DS, Zaretsky JM, Escuin-Ordinas H, *et al*. Primary resistance to PD-1 blockade mediated by JAK1/2 mutations. *Cancer Discov* 2017;7:188–201.
52 Sucker A, Zhao F, Pieper N, *et al*. Acquired IFNγ resistance impairs anti-tumor immunity and gives rise to T-cell-resistant melanoma lesions. *Nat Commun* 2017;8:15440.
53 Benci JL, Johnson LR, Choa R, *et al*. Opposing functions of interferon coordinate adaptive and innate immune responses to cancer immune checkpoint blockade. *Cell* 2019;178:933–48.
54 Rocamora-Reverte L, Reichardt HM, Villunger A, *et al*. T-Cell autonomous death induced by regeneration of inert glucocorticoid metabolites. *Cell Death Dis* 2017;8:e2948.
55 Chuanxin Z, Shengzheng W, Lei D, *et al*. Progress in 11β-HSD1 inhibitors for the treatment of metabolic diseases: a comprehensive guide to their chemical structure diversity in drug development. *Eur J Med Chem* 2020;191:S0223-5234(20)30101-X.
56 Kennedy LB, Salama AKS. A review of immune-mediated adverse events in melanoma. *Oncol Ther* 2019;7:101–20.
57 Ramos-Casals M, Brahmer JR, Callahan MK, *et al*. Immune-related adverse events of checkpoint inhibitors. *Nat Rev Dis Primers* 2020;6:38.